

Article

Investigating the Catalytic Deactivation of a Pd Catalyst during the Continuous Hydrogenation of CO₂ into Formate Using a Trickle-Bed Reactor

Kwangho Park ¹, Kyung Rok Lee ¹, Sunghye Ahn ^{1,2}, Hongjin Park ³, Seokyeong Moon ³ , Sungho Yoon ³ and Kwang-Deog Jung ^{1,2,*} 

¹ Clean Energy Research Center, Korea Institute of Science and Technology, 5, Hwarang-ro 14-gil, Seongbuk-gu, Seoul 02792, Republic of Korea; kwangho@kist.re.kr (K.P.); lkr2003@kist.re.kr (K.R.L.); 023854@kist.re.kr (S.A.)

² Division of Energy & Environmental Technology, KIST School, Korea National University of Science and Technology, Seoul 02792, Republic of Korea

³ Department of Chemistry, Chung Ang University (CAU), 84 Heukseok-ro, Dongjak-gu, Seoul 06974, Republic of Korea; phj1553@gmail.com (H.P.); mmm0503@cau.ac.kr (S.M.); sunghoyoon@cau.ac.kr (S.Y.)

* Correspondence: jkdcatal@kist.re.kr; Tel.: +82-958-5218

Abstract: The practical application of formic acid production through the hydrogenation of CO₂ has garnered significant attention in efforts to tackle the challenges associated with (1) achieving net-zero production of formic acid as a chemical feedstock and (2) improving hydrogen storage and transport. This study focuses on demonstrating the continuous operation of a trickle bed reactor for converting CO₂ into formate using palladium on activated carbon (Pd/AC). Optimal temperature conditions were investigated through a dynamic operation for 24 h, achieving the maximum productivity of 2140 mmol_{FA}·g_{Pdsurf}⁻¹·h⁻¹ at 150 °C and 8 MPa, with an H₂/CO₂ ratio of 1:1; however, catalyst deactivation was observed in the process. Stability tests performed under continuous operation at 120 °C and 8 MPa with an H₂/CO₂ ratio of 1:1 indicated a gradual decline in productivity, culminating in a 20% reduction after 20 h. A comprehensive analysis comparing fresh and spent catalysts revealed that the diminished catalytic activity at elevated temperatures was attributed to the partial sintering and leaching of Pd nanoparticles during the hydrogenation process. These findings offer insights for the future development of novel Pd-based catalyst systems suitable for continuous hydrogenation processes.

Keywords: CO₂ hydrogenation; formic acid; heterogeneous catalyst; palladium; continuous process



Citation: Park, K.; Lee, K.R.; Ahn, S.; Park, H.; Moon, S.; Yoon, S.; Jung, K.-D. Investigating the Catalytic Deactivation of a Pd Catalyst during the Continuous Hydrogenation of CO₂ into Formate Using a Trickle-Bed Reactor. *Catalysts* **2024**, *14*, 187. <https://doi.org/10.3390/catal14030187>

Academic Editor: Junling Lu

Received: 14 February 2024

Revised: 28 February 2024

Accepted: 29 February 2024

Published: 9 March 2024



Copyright: © 2024 by the authors. Licensee MDPI, Basel, Switzerland. This article is an open access article distributed under the terms and conditions of the Creative Commons Attribution (CC BY) license (<https://creativecommons.org/licenses/by/4.0/>).

1. Introduction

The urgent need for eco-friendly energy and chemical production driven by rapid climate change has spotlighted CO₂ hydrogenation to formic acid and its derivatives [1–3]. This approach not only repurposes emitted CO₂ but also offers an efficient hydrogen storage solution [4–7]. Recent successes in the use of formic acid as a fuel cell energy source in public transport have highlighted its potential as a hydrogen-based economy [8]. Moreover, recent LCA-TEA reports highlight the positive impact of CO₂-hydrogenated formate (FA) production in thermo- or electrochemical catalytic systems, especially with the rapidly emerging technology for the integration of renewable energy [9–14]. Electrochemical systems for producing formate are gaining prominence because of their efficient integration with renewable energy sources and their potential to significantly reduce the impact of global warming, showcasing promising electrolyzer performance [15–17]. However, the scalability of these systems to continuously produce concentrated formate and the cost implications of the separation process require further development. The thermo-catalytic systems face challenges in terms of economic aspects, such as high reactant costs,

significant energy demands for purification, and lower catalytic efficiencies, hindering their competitiveness against traditional fossil fuel-based processes. The development of efficient catalytic systems is crucial for enhancing process efficiency from an economic standpoint. Intensive research has focused on various catalytic systems, with a significant emphasis on heterogeneous catalyst systems, which offer numerous advantages, such as easy separation from the reaction medium [3,18–22]. Among these, Pd-based catalytic systems have demonstrated exceptional performance [23,24]. However, most studies have focused on simple batch reactions using Pd-based catalyst systems. However, for practical applications in industrial processes, a thorough investigation of catalytic systems in feasible reactor types is also essential to realize the full potential of the CO₂-hydrogenated FA production process.

Trickle-bed reactors are multiphase reactors with continuous and co-current flows of liquid (in the downward direction) and gas (in the upward or downward direction) reactants over a stationary (or fixed) solid catalyst. Throughout the history of industrial processes, trickle-bed reactor systems have typically been used in diverse sectors such as petroleum, fine chemicals, and biochemical fields, particularly contributing to hydrogenation and hydrodesulfurization in refineries owing to various advantages such as facile installments, minimal catalyst loading, and ease of catalyst separation [25,26]. From this perspective, trickle-bed reactors show potential for the mass production of CO₂-based formic acid by hydrogenation. Building on this, our research team developed a Ru catalyst supported on a covalent triazine framework and demonstrated its exceptional stability through long-term performance evaluations using a trickle-bed reactor system [27–29]. Although extensive research is ongoing, the feasibility of Pd catalysts must be proven during continuous process operations.

In this study, we investigated the continuous hydrogenation of CO₂ to FA using a commercially available palladium on activated carbon (Pd/AC) catalyst in a trickle-bed reactor system. This study is the first attempt to assess the feasibility of using a Pd catalyst in such a system through dynamic operations at varying reaction temperatures. In particular, we analyzed the deactivation behavior of the Pd catalysts during extended continuous tests. Through comprehensive characterization, we aimed to elucidate the causes of the decreased catalytic activity and provide insights into the continuous application of Pd-based catalysts.

2. Results and Discussion

2.1. Continuous Hydrogenation of CO₂ to Formate over Trickle-Bed Reactor

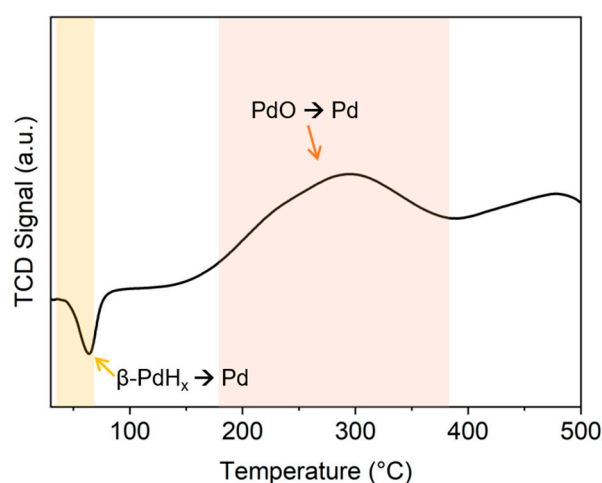
2.1.1. Preliminary Analysis on the Fresh Pd/AC Catalyst

Before continuous hydrogenation, inductively coupled plasma optical emission spectrometry (ICP-OES) was performed to determine Pd loading in the Pd/AC catalyst (Table 1). The results revealed a Pd content of 4.45 wt% for the fresh Pd/AC catalyst. Given this result, the catalytic activity of the catalyst during the continuous process was quantified using formate productivity, which represents the moles of formate produced per mole of surface-exposed Pd metal determined by the CO-chemisorption per hour. Further, H₂ temperature-programmed reduction (H₂-TPR) was performed to understand the redox property of the supported Pd species on the Pd/AC catalyst (Figure 1). Pd-based catalysts absorb hydrogen even under ambient conditions and readily form palladium hydride (PdH_x). Consequently, the first negative peak at 63 °C indicates the decomposition of PdH_x generated by the hydrogen absorption of Pd nanoparticles at the ambient temperature [30,31]. The result also revealed that the reduction in PdO species began at approximately 150 °C and completed at approximately 400 °C. Considering this, the reduction condition for the Pd/AC catalyst bed was determined to be 300 °C for 3 h. Additionally, the dispersity of the Pd species was determined by the CO chemisorption, giving a Pd dispersion of 29.4% with a mean diameter of 3.82 nm.

Table 1. Characterization results on the fresh Pd/AC through ICP-OES, CO-chemisorption, and N₂ adsorption and desorption isotherm analysis.

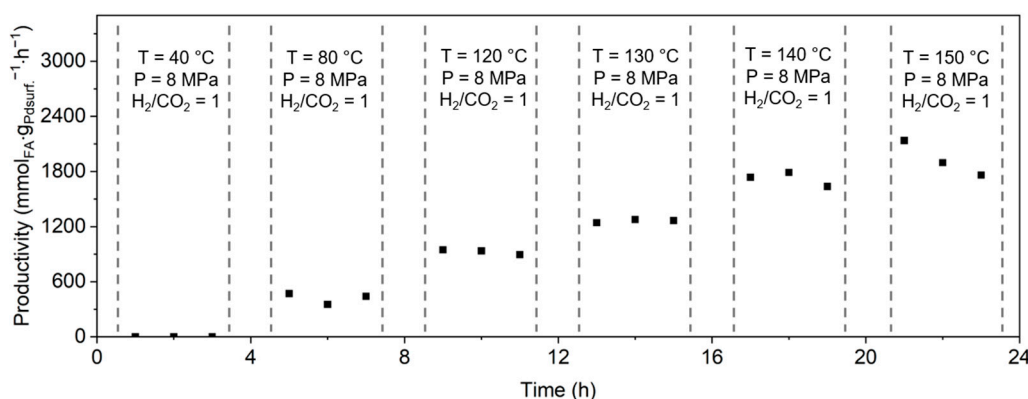
Sample	Pd Content ^a (wt%)	D ^b (%)	d ^b (nm)	S _A BET ^c (m ² g ⁻¹)	V _{pore} ^c (cm ³ g ⁻¹)	d _{mean} ^c (nm)
Fresh Pd/AC	4.45	29.4	3.82	1000	0.53	2.13
Spent Pd/AC	3.25	26.9	4.15	1090	0.61	2.24

^a Pd content was determined by ICP-OES analysis. ^b Dispersity (D) and mean particle size (d) of the Pd species were obtained from CO-chemisorption. ^c Porosity parameters were calculated based on N₂ adsorption and desorption analyses using the Teller (BET) method.

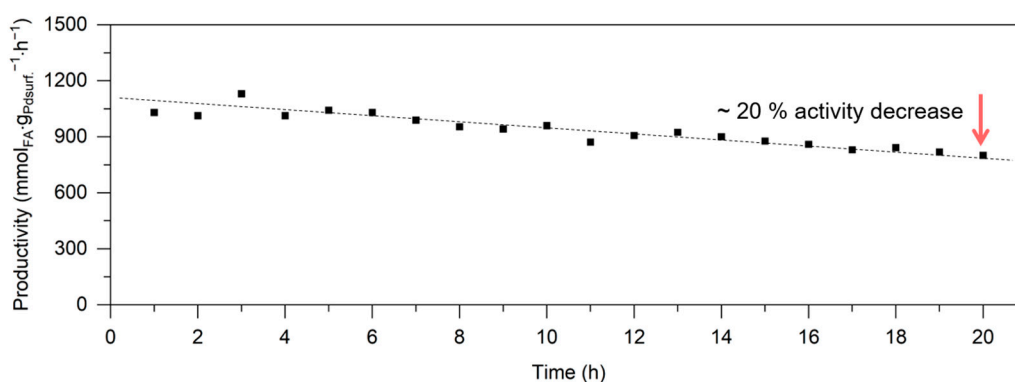
**Figure 1.** H₂-TPR analysis on fresh Pd/AC catalyst.

2.1.2. Dynamic Operation with a Variation of Reaction Temperature

Figure 2a presents the results of the dynamic hydrogenation of CO₂ to formate in a trickle-bed reactor utilizing a Pd/AC catalyst. To observe the temperature-dependent catalytic activity and reaction behavior, the temperature of the trickle-bed reaction was incrementally varied from a mild condition of 40 °C up to 150 °C. The Pd/AC catalyst bed was fixed axially in the middle of the reactor and, before the reaction, was subjected to a reduction process at 300 °C, aimed at eliminating any oxidation that may have occurred on the catalyst surface when exposed to the atmosphere. The reaction feed for the trickle-bed reactor system, such as CO₂, H₂O, or Et₃N, was continuously supplied to the top of the reactor using high-pressure liquid pumps, whereas the flow of H₂ gas was controlled by a mass flow controller. During this process, the reaction was conducted under a constant pressure of 8 MPa, and the superficial velocity of CO₂ was maintained at 1.67 cm·s⁻¹. At a low temperature of 40 °C, the Pd/AC catalyst demonstrated negligible catalytic activity. However, a notable enhancement in catalytic efficiency was observed when the temperature range was extended from 80 to 150 °C. Within this temperature range, the average FA production over 3 h escalated from 420 to 1930 mmol_{FA}·g_{Pd surf.}⁻¹·h⁻¹. Correspondingly, the average turnover frequencies (TOF_{avg.}) showed an increase from 45 to 205 h⁻¹. However, a discernible decline in productivity was observed when the system was operated at 150 °C for 3 h. Therefore, a temperature setting of 120 °C was identified as the most favorable for subsequent operations. After dynamic operation, the stability of continuous hydrogenation in the trickle-bed reactor system was evaluated for 20 h (Figure 2b). The result confirms the promising stability; however, a gradual decrease in the catalytic activity from 1030 to 800 mmol_{FA}·g_{Pd surf.}⁻¹·h⁻¹ was observed. To determine the underlying principle of the decline in catalytic activity, nitrogen adsorption and desorption, X-ray photoelectron spectroscopy (XPS), transmittance electron microscopy (TEM), and X-ray absorption spectroscopy (XAS) were used to analyze the changes in the physicochemical properties of the fresh and spent catalysts.



(a)



(b)

Figure 2. (a) Dynamic operation with a variation of the reaction temperature and (b) 20 h stability assessment for the CO₂ hydrogenation to formate using Pd/AC catalyst.

2.2. Comprehensive Characterizations by the Comparison of Fresh and Spent Catalysts

2.2.1. N₂ Adsorption and Desorption Analysis

To elucidate the alterations in the pore structure of the Pd/AC catalyst, N₂ adsorption–desorption isotherms were obtained for both fresh and spent catalysts, as depicted in Figure 3. The fresh Pd/AC catalyst displayed a notable adsorption onset at $p/p_0 < 0.1$, which is characteristic of type I and II isotherms (Figure 3a) [32]. This pattern suggests the predominance of micropores within the activated carbon support. By contrast, the isotherm profile of the catalyst recovered post-20-hour hydrogenation (Figure 3b) reveals a trend similar to that of the fresh catalyst, indicating that the pore structure remains largely unchanged throughout the reaction. The t-plot curves for both the fresh and spent catalysts, shown in Figure 3c,d, demonstrate a sharp increase in the adsorption volume in the lower p/p_0 region up to 0.3, featuring a micropore volume of $0.398 \text{ cm}^3 \text{ g}^{-1}$ for the fresh catalyst and $0.427 \text{ cm}^3 \text{ g}^{-1}$ for the spent catalyst. This indicates considerable adsorption within the micropore structure. Moreover, the Brunauer–Emmett–Teller (BET) specific surface areas of the fresh and spent Pd/AC catalysts were 1002 and $1095 \text{ m}^2 \text{ g}^{-1}$, respectively, which were strikingly similar (as listed in Table 1). Hence, it was evident that the pore structure of the catalyst underwent minimal alteration during continuous hydrogenation.

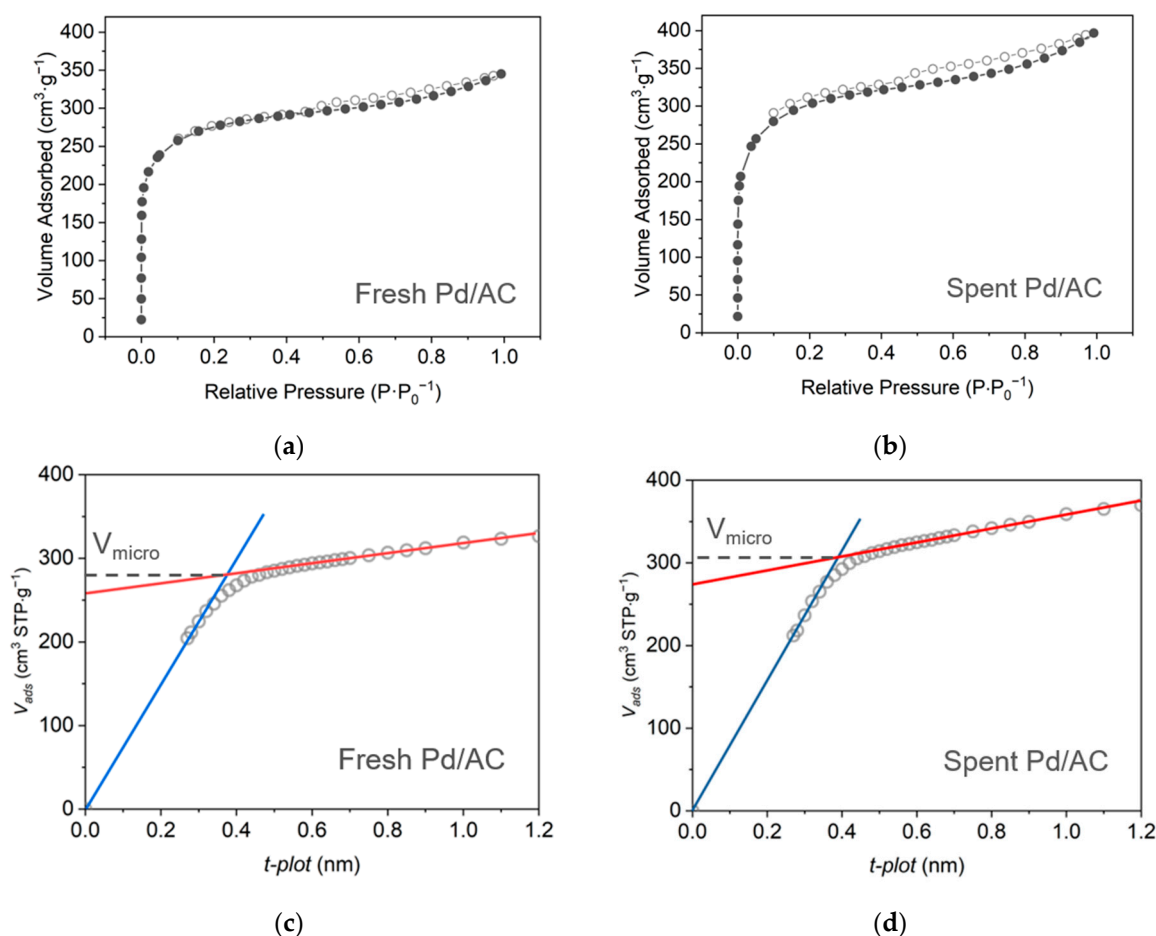


Figure 3. N₂ adsorption–desorption isotherms (solid circle: adsorption, hollow circle: desorption) for (a) fresh Pd/AC and (b) spent Pd/AC, determination of micropore volume using t-plot method for (c) fresh Pd/AC and (d) spent Pd/AC catalysts.

2.2.2. Transmittance Electron Microscope Analysis

Variations in the dispersion state of the Pd species supported on the catalyst were investigated using high-resolution transmission electron microscopy (HR-TEM), comparing fresh and spent catalyst samples (Figure 4a,b). For both catalysts, a substantial distribution of Pd nanoparticles was observed across the support structure. Fast Fourier transform (FFT) analysis of the high-angle annular dark-field scanning transmission electron microscopy (HAADF-STEM) images revealed that the lattice fringe d-spacing of the fresh catalyst was 2.26 Å, aligned with the (111) plane of the face-centered cubic (fcc) lattice structure of metallic Pd [33]. By contrast, the spent catalyst exhibits a lattice fringe d-spacing of 1.90 Å, corresponding to the (200) plane of the metallic Pd species. However, particle size distribution (PSD) analysis highlighted the differences between the two catalysts. The mean PSD of the Pd nanoparticles in the fresh catalyst is 3.74 nm, whereas that of the spent catalyst increased to 4.02 nm. This suggests that the Pd nanoparticles undergo partial sintering under reductive hydrogenation conditions.

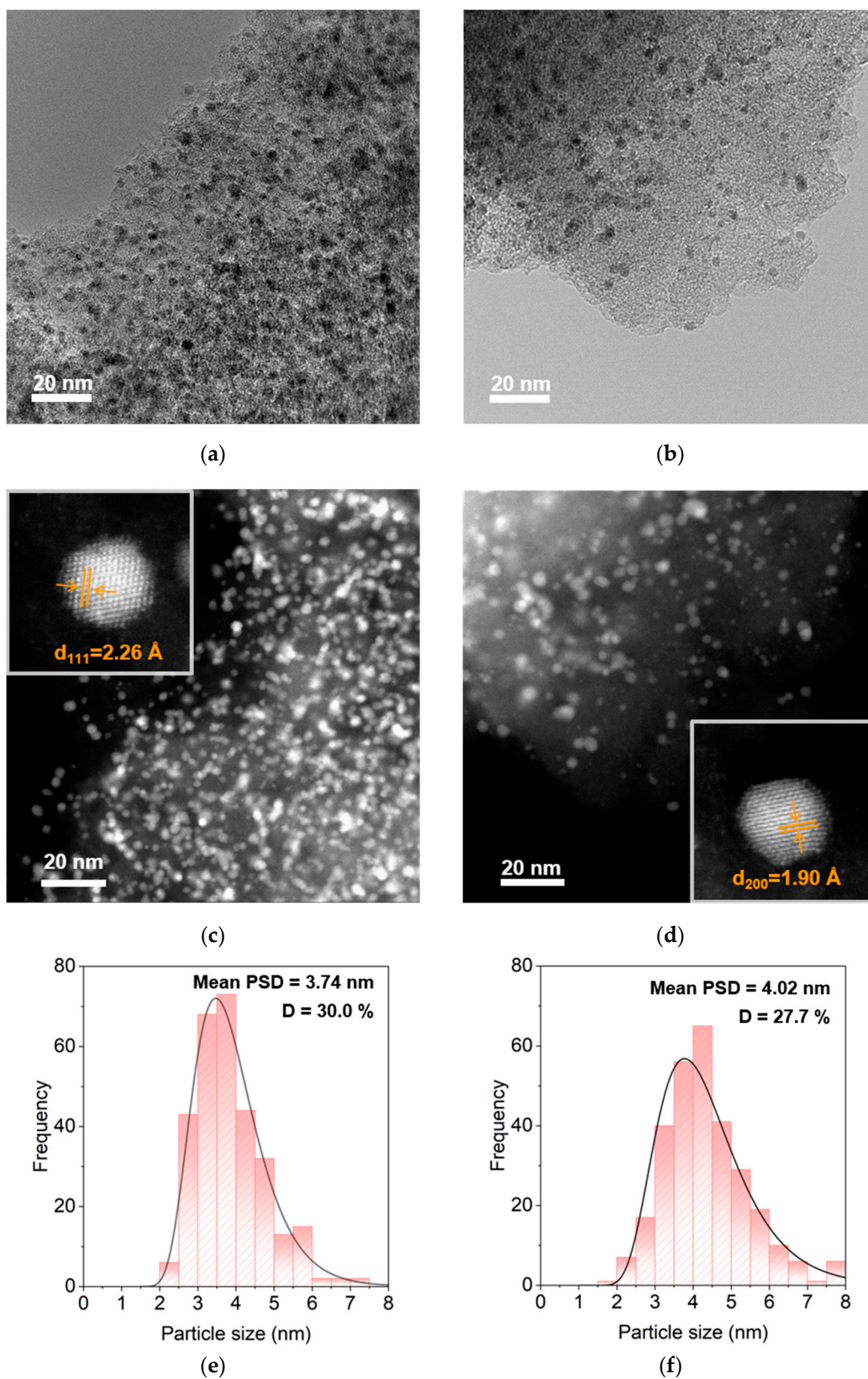


Figure 4. HR-TEM images of (a) fresh Pd/AC and (b) spent Pd/AC catalyst. HAADF-STEM images and FFT analysis (inset) of (c) fresh Pd/AC and (d) spent Pd/AC catalyst. Particle size distribution analysis on (e) fresh Pd/AC and (f) spent Pd/AC catalyst.

2.2.3. X-ray Diffraction Analysis

The microstructural characteristics of the fresh and spent Pd/AC catalysts were meticulously analyzed using wide-angle X-ray diffraction (XRD) to gain insight into the crystallinity of the support materials and the phase change of the supported Pd species (Figure 5). The XRD analysis results, as shown in Figure 5, show distinct patterns that are crucial for understanding the structural properties of the catalysts. The patterns feature broad and low-intensity peaks at 2θ values of approximately 23° and 42° . These angles correspond to the (002) and (100) planes of carbon, respectively. The broadness and low intensity of these peaks suggest the amorphous nature of the carbon material, highlighting the lack of long-range crystalline order that is typically associated with graphitic structures. Furthermore, the analysis revealed distinct and strong peaks at 2θ values of approximately 40° and 47° , marked with diamonds in the figure. These peaks are attributed to the (111) and (200) planes of the metallic Pd species, respectively. The presence of these peaks is consistent with the TEM results. Furthermore, diffraction peaks at 2θ values of 34° and 43° were observed (marked with circles), indicating the presence of PdO species in the fresh catalyst. XRD analysis revealed notable changes in the Pd/AC catalyst before and after use. Specifically, an increase in the intensity of peaks at 2θ values of 40° and 47° and disappearance of the peaks at 34° and 43° were observed for the spent Pd/AC catalyst in comparison to the fresh catalyst. This increase in peak intensity is a clear indication of the sintering of the supported Pd nanoparticles, which suggests that these nanoparticles coalesced into larger particles and simultaneously reduced the PdO species during the continuous hydrogenation process.

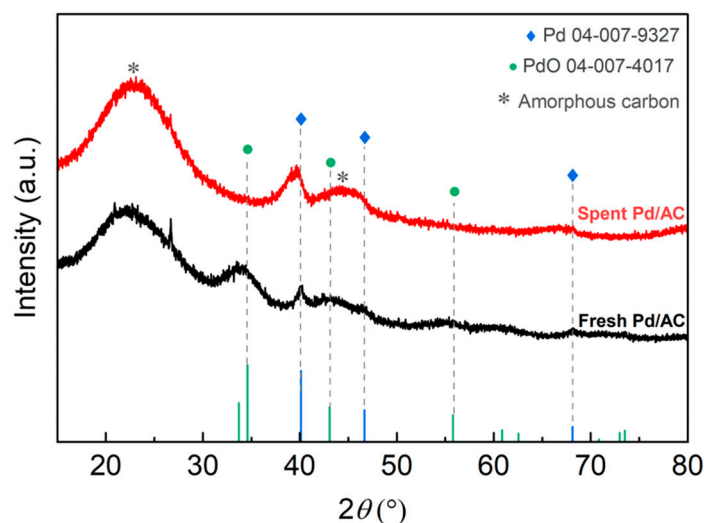


Figure 5. XRD analysis for the fresh and spent Pd/AC catalysts.

2.2.4. X-ray Photoelectron Spectroscopy Analysis

The oxidation states of the Pd species in both the fresh and spent catalysts were meticulously examined using X-ray photoelectron spectroscopy (XPS), which provided a crucial understanding of the chemical environment and electronic structure of the catalysts, as shown in Figure 6. The detailed C1s XPS spectra of the fresh and spent Pd/AC catalysts are shown in Figure 6a,b, respectively. The spectra reveal multiple peaks at the binding energies of 284.8, 286.3, 287.4, 289.0, and 291.0 eV, which correspond to various carbon bonds: C–C/C–H (indicative of graphitic or hydrocarbon structures), C–O (alcohol or ether functionalities), C=O (carbonyl groups), C–O=O (carboxylate groups), and $\pi - \pi^*$ transitions (associated with conjugated or aromatic systems), respectively. Furthermore, the analysis of the Pd 3d_{5/2} XPS spectrum of the fresh Pd/AC catalyst, presented in Figure 6c, reveals two distinct peaks. These peaks correspond to the metallic palladium (Pd⁰) at a binding energy range of 335.7–336.1 eV and palladium in a +2 oxidation state (Pd²⁺) at

a range of 337.3–338.1 eV [34,35]. The presence of these peaks indicates the coexistence of metallic and oxidized forms of Pd on the catalyst surface. Notably, the intensity of the peak associated with Pd²⁺ was significantly higher than that of Pd⁰, with a ratio of approximately 2.8:1, suggesting the predominance of oxidized PdO species. This oxidation is likely due to exposure to atmospheric conditions during catalyst preparation or storage. Conversely, the spent Pd/AC catalyst exhibited a notable shift in the Pd 3d_{5/2} XPS profile (Figure 6d). This shift was characterized by a significant change in the ratio of Pd²⁺ to Pd⁰, which changed to 0.19:1. This dramatic shift indicated the reduction in the PdO species to a more metallic state under the reductive conditions of the hydrogenation process. This observation is in line with the partial sintering of the Pd nanoparticles, as evidenced by the TEM and XRD analyses.

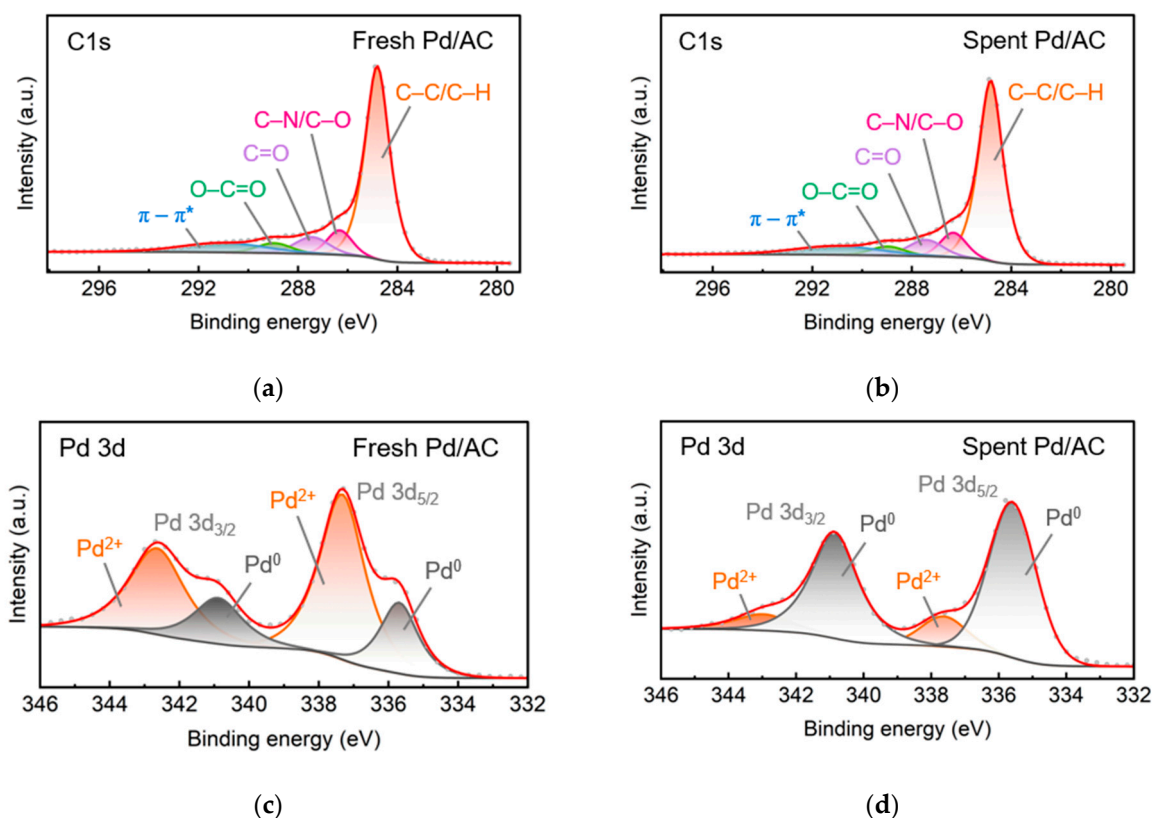


Figure 6. Deconvoluted C1s XPS spectra of (a) fresh Pd/AC and (b) spent Pd/AC. Deconvoluted Pd 3d XPS spectra of (c) fresh Pd/AC and (d) spent Pd/AC.

2.2.5. X-ray Absorption Spectroscopy Analysis

Figure 7 illustrates the findings from the X-ray absorption spectroscopy (XAS) analysis conducted on both the fresh and spent catalysts. This analysis provided precise insights into the electronic properties and coordination characteristics of the supported Pd species with exceptional sensitivity. The X-ray absorption near edge structure (XANES) spectra showed that the energy absorption thresholds for both the fresh and spent Pd/AC catalysts were closely aligned with that of the Pd foil reference (Figure 7a). This observation indicates that the supported Pd species were primarily in a metallic state with a Pd⁰ oxidation state [36]. Figure 7b shows the extended X-ray absorption fine structure (EXAFS) spectra of the Pd/AC catalysts. The EXAFS spectra revealed peaks corresponding to Pd–O and Pd–Pd at radial distances of 1.48–1.51 Å and 2.48–2.51 Å, respectively. A notable decrease in the intensity of the Pd–O coordination for the spent Pd/AC catalyst was observed following continuous hydrogenation, suggesting the reduction and partial sintering of the Pd nanoparticles. This inference is further substantiated by fitting analyses using the Pd–O and Pd–Pd contributions derived from the reference materials (Figure 8a–d). For

the fresh Pd/AC catalyst, the coordination numbers (CN) were determined to be 1.78 for the Pd–O bond and 3.83 for the Pd–Pd bond (Table 2). In comparison, the spent Pd/AC catalyst exhibited altered CN values, with 0.91 for the Pd–O bond and 6.09 for the Pd–Pd bonds. These results demonstrate a reduction in the Pd–O component of the spent catalyst, attributable to the hydrogenation process. Additionally, the increased CN for the Pd–Pd bond indicates post-reaction sintering of the Pd nanoparticles.

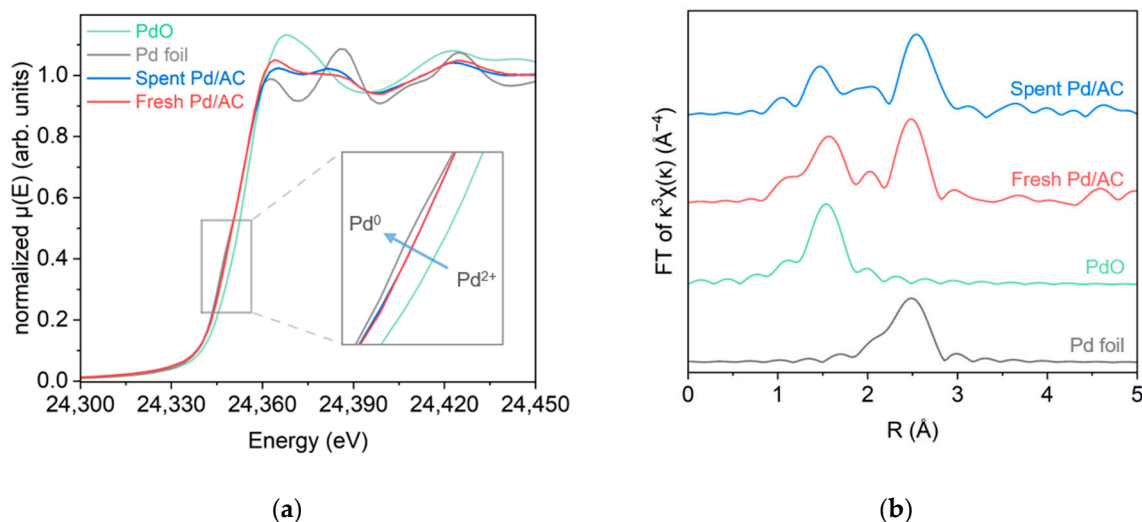


Figure 7. XAS characterization. (a) Normalized Pd K-edge XANES spectra and (b) EXAFS profiles of fresh and spent Pd/AC catalysts in the comparison with Pd foil and PdO references.

Based on the results of a continuous carbon dioxide hydrogenation reaction using a trickle-bed reactor and an in-depth analysis of the catalyst recovered after the reaction, this study confirmed that the activity of the Pd/AC catalyst gradually decreased over long reaction durations. This decline in activity was attributed to the leaching of Pd nanoparticles owing to the continuous feed flow and sintering caused by exposure to a reducing environment. The sintering of the nanoparticles due to leaching and reduction results in irreversible deactivation, which cannot be reversed by catalyst regeneration. Therefore, from a practical perspective, this catalyst is not suitable for long-term reactions. The fundamental reason for these outcomes is believed to be the limitations of the activated carbon supports. Recent trends in the research on FA production through carbon dioxide hydrogenation have shown that in catalyst systems based on Pd and various single-atom catalysts, strong interactions between the support surface and supported metals significantly enhance the stability of the supported metal catalysts under reducing conditions [37–44]. Furthermore, catalyst supports based on metal oxides and organic materials improve the stability of catalysts during hydrogenation reactions by confining the Pd nanoparticles within their unique pore structures. Continuous hydrogenation reactions have the advantage of being simple and operable under scalable conditions within a thermodynamic conversion system. However, the process still faces challenges, such as low reaction efficiency owing to the continuous reaction feed flow and short residence time. As discussed previously, the development of innovative synthetic methods that can precisely control the chemical state of a support surface is crucial. Simultaneously, developing supports that can effectively confine Pd nanoparticles within a costructure while enhancing the mass transfer efficiency of the reactants is of great importance.

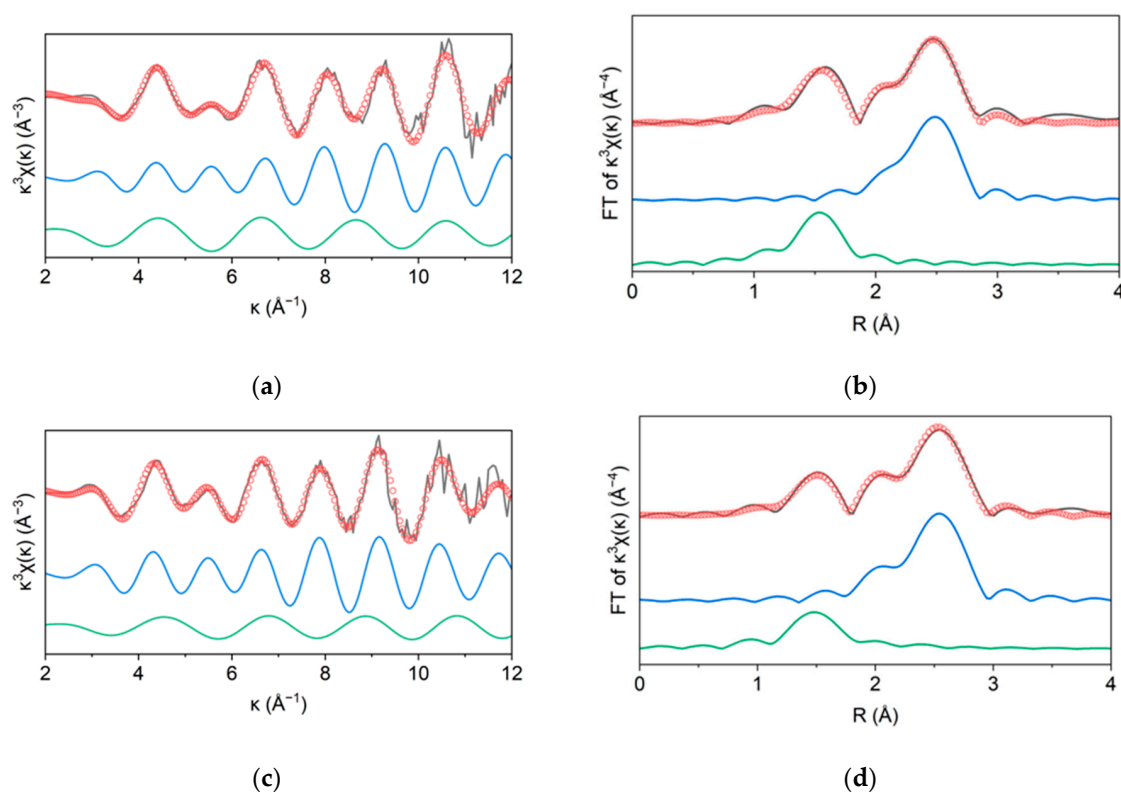


Figure 8. Curve fitting of EXAFS oscillations. (a) Pd K-edge EXAFS oscillation for fresh Pd/AC, (b) FT spectra of fresh Pd/AC, (c) Pd K-edge EXAFS oscillation for spent Pd/AC, (d) FT spectra of spent Pd/AC (black line: experimental data, red dot: fit, blue line: Pd foil data, and green line: PdO data).

Table 2. Details of the EXAFS fitting parameters.

Sample	Bond	CN	R (\AA)	σ^2 (\AA^2)	E_0 (eV)
Fresh Pd/AC	Pd-O	1.78	2.01 ± 0.02	0.0015	2.737
	Pd-Pd	3.83	2.74 ± 0.02	0.0071	-2.432
Spent Pd/AC	Pd-O	0.91	1.98 ± 0.02	0.0010	2.858
	Pd-Pd	6.09	2.77 ± 0.01	0.0098	-1.725

3. Materials and Methods

3.1. Materials

Pd/AC catalyst was purchased from Sigma-Aldrich, St Louis, MO, USA and used without further purification. Triethylamine (>99%) were procured from Samchun Pure Chemical Company, Pyeongtaek, Republic of Korea. Double-distilled water was used in all experiments. All the gases (99.99% in purity) used in this study were supplied by Shinyang Company, Seoul, Republic of Korea.

3.2. Characterization Methods

H_2 temperature-programmed reduction (H_2 -TPR) and CO-chemisorption analyses were performed using a BELCAT II (MicrotracBEL Corp, Osaka, Japan). For H_2 -TPR, we utilized a 5% H_2 /Ar carrier gas at a flow rate of $30 \text{ mL}\cdot\text{min}^{-1}$, with temperature increasing from 40 to $650 \text{ }^\circ\text{C}$ at $10 \text{ }^\circ\text{C}\cdot\text{min}^{-1}$. Prior to analysis, samples were dried at $150 \text{ }^\circ\text{C}$ for an hour under argon flow. For CO-chemisorption, samples underwent pretreatment with a 5% H_2 /Ar mixture at $300 \text{ }^\circ\text{C}$ for 1 h at $50 \text{ mL}\cdot\text{min}^{-1}$ flow rate, followed by CO adsorption using a 10% CO/He mixture at $25 \text{ }^\circ\text{C}$ through pulse injection over eight cycles. Sample preparation for ICP involved the Ethos 1 system, with Pd quantification performed using

an Avio 500 ICP-OES analyzer (Perkin-Elmer, Boston, MA, USA). TEM imaging and EDS mapping were conducted on a TEM-Talos (F200X) operating at 200 kV with a LaB6 source. Line-profile analysis was carried out using a TEM-Tecnai (F20 G2) at 50 to 200 kV, offering less than 23 nm resolution and 25 to 1,030,000 \times magnification. High-resolution STEM images of Pd nanoparticles were obtained from a double Cs-corrected Titan Themis TEM (FEI; TitanTM 80-300). N₂ adsorption/desorption isotherms were analyzed using a BEL sorp mini II system, with surface areas calculated via the Brunauer–Emmett–Teller (BET) method. XPS measurements were performed on a PHI 5000 Versa Probe spectrometer (Ulvac-PHI, Chigasaki, Japan) using a monochromatized Al K α source. HPLC analysis was conducted with a YL 9100 Plus system (YL Instruments Co., Ltd. Seoul, South Korea), featuring a RI detector and an Aminex HPX-87H column, operated at 50 °C with a 5 mM H₂SO₄ eluent at 0.6 mL \cdot min⁻¹ flow rate. XAFS spectra were collected at the Pohang Accelerator Laboratory (PLS-II, 3.0 GeV, Pohang, South Korea) 10C Wide XAFS beamline, analyzed using Demeter 0.9.26 software, and EXAFS fitting was performed with an S₀² value of 0.791 to determine coordination numbers.

3.3. Continuous Hydrogenation of CO₂ to Formate over Trickle-Bed Reactor

The continuous hydrogenation process was carried out in a custom-built stainless-steel bar reactor. Inside the reactor, Pd/AC was positioned centrally, with glass wool and beads filling the remaining space. The reactor was pressurized to 8 MPa with 1:1 ratio of H₂ and CO₂, and the temperature was raised up to the targeted temperature of 40 and 150 °C using an electric furnace. A back-pressure regulator maintained the pressure at the set temperature, while a mass flow controller regulated the H₂ gas flow. Liquid CO₂ from a siphon cylinder was controlled via a high-pressure liquid pump and vaporized before entering the reactor through a heated line. Distilled water and Et₃N were also supplied to the reactor using another high-pressure liquid pump. The liquid products were collected and analyzed using high-performance liquid chromatography. The FA productivity and surface exposed Pd content were then calculated using Equations (1) and (2). After the reaction, the spent catalyst was retrieved from the reactor and washed with water (100 mL \times 3) through filtration. Then, the recovered catalyst was dried under vacuum at 80 °C before further characterization.

$$\text{Formate productivity} \left(\text{mmol}_{\text{FA}} \cdot \text{g}_{\text{Pd surf.}}^{-1} \cdot \text{h}^{-1} \right) = \frac{\text{production rate of HCOO}^- \left(\text{mmol}_{\text{FA}} \cdot \text{h}^{-1} \right)}{\text{Surface exposed Pd content} \left(\text{g}_{\text{Pd surf.}} \right)} \quad (1)$$

$$\text{Surface exposed Pd content} \left(\text{g}_{\text{Pd surf.}} \right) = \text{Pd content} \left(\text{g} \right) \times \frac{\text{Dispersity of Pd} \left(\% \right)}{100 \left(\% \right)} \quad (2)$$

4. Conclusions

This study successfully demonstrates the viability of using a Pd/AC catalyst in a trickle-bed reactor for the continuous hydrogenation of CO₂ to formate. Optimal operating conditions were established, with the reactor achieving maximum FA productivity at 150 °C and 8 MPa. However, the most favorable operating temperature was identified as 120 °C, where a balance between productivity and catalyst stability was observed. Over time, a gradual decrease in catalytic activity was noted, with a 20% reduction after 20 h of continuous operation. Detailed analyses, including HR-TEM, XPS, TEM, and XAS, provided insights into the physicochemical changes in the catalyst. These analyses revealed that deactivation of the catalyst, primarily due to partial sintering and leaching of Pd nanoparticles, was a key factor affecting the performance. Furthermore, the study confirmed the presence of metallic Pd species in both fresh and spent catalysts, with a notable shift in the coordination numbers after the reaction. These findings are instrumental in guiding the development of more efficient Pd-based catalyst systems for sustainable formic acid production, highlighting the importance of catalyst stability and optimization of operating conditions in continuous processes.

Author Contributions: K.P.: Conceptualization, formal analysis, investigation, writing—original draft, writing—review and editing. K.R.L. and S.A.: Data curation, validation. H.P. and S.M.: Data curation. S.Y.: Project administration, resources. K.-D.J.: Conceptualization, funding acquisition, project administration, resources, supervision. All authors have read and agreed to the published version of the manuscript.

Funding: This work was supported by the Korea Institute of Science and Technology (KIST), the Carbon to X Project (2020M3H7A1096360) through the National Research Foundation (NRF) (Ministry of Science and ICT, Republic of Korea), and was also financially supported by the Methanol Project (20225A10100090) through the Korea Institute of Energy Technology Evaluation and Planning (KETEP) (Ministry of Trade, Industry and Energy, Republic of Korea).

Data Availability Statement: All data are available in the main text.

Acknowledgments: X-ray absorption spectral measurements were supported by the 10C beamline of the Pohang Accelerator Laboratory (Republic of Korea) under contact No. 2023-1st-10C-087.

Conflicts of Interest: The authors declare no conflicts of interest.

References

1. Sordakis, K.; Tang, C.; Vogt, L.K.; Junge, H.; Dyson, P.J.; Beller, M.; Laurenczy, G. Homogeneous catalysis for sustainable hydrogen storage in formic acid and alcohols. *Chem. Rev.* **2018**, *118*, 372–433. [[CrossRef](#)] [[PubMed](#)]
2. Wang, W.-H.; Himeda, Y.; Muckerman, J.T.; Manbeck, G.F.; Fujita, E. CO₂ hydrogenation to formate and methanol as an alternative to photo- and electrochemical CO₂ reduction. *Chem. Rev.* **2015**, *115*, 12936–12973. [[CrossRef](#)] [[PubMed](#)]
3. Álvarez, A.; Bansode, A.; Urakawa, A.; Bavykina, A.V.; Wezendonk, T.A.; Makkee, M.; Gascon, J.; Kapteijn, F. Challenges in the greener production of formates/formic acid, methanol, and DME by heterogeneously catalyzed CO₂ hydrogenation processes. *Chem. Rev.* **2017**, *117*, 9804–9838. [[CrossRef](#)] [[PubMed](#)]
4. Enthaler, S.; von Langermann, J.; Schmidt, T. Carbon dioxide and formic acid—The couple for environmental-friendly hydrogen storage? *Energy Environ. Sci.* **2010**, *3*, 1207–1217. [[CrossRef](#)]
5. Loges, B.; Boddien, A.; Gärtner, F.; Junge, H.; Beller, M. Catalytic generation of hydrogen from formic acid and its derivatives: Useful hydrogen storage materials. *Top. Catal.* **2010**, *53*, 902–914. [[CrossRef](#)]
6. Grasemann, M.; Laurenczy, G. Formic acid as a hydrogen source—recent developments and future trends. *Energy Environ. Sci.* **2012**, *5*, 8171–8181. [[CrossRef](#)]
7. Mellmann, D.; Sponholz, P.; Junge, H.; Beller, M. Formic acid as a hydrogen storage material—development of homogeneous catalysts for selective hydrogen release. *Chem. Soc. Rev.* **2016**, *45*, 3954–3988. [[CrossRef](#)] [[PubMed](#)]
8. van Putten, R.; Wissink, T.; Swinkels, T.; Pidko, E.A. Fuelling the hydrogen economy: Scale-up of an integrated formic acid-to-power system. *Int. J. Hydrogen Energy* **2019**, *44*, 28533–28541. [[CrossRef](#)]
9. Otto, A.; Grube, T.; Schiebahn, S.; Stolten, D. Closing the loop: Captured CO₂ as a feedstock in the chemical industry. *Energy Environ. Sci.* **2015**, *8*, 3283–3297. [[CrossRef](#)]
10. Pérez-Fortes, M.; Schöneberger, J.C.; Boulamanti, A.; Harrison, G.; Tzimas, E. Formic acid synthesis using CO₂ as raw material: Techno-economic and environmental evaluation and market potential. *Int. J. Hydrogen Energy* **2016**, *41*, 16444–16462. [[CrossRef](#)]
11. Sternberg, A.; Jens, C.M.; Bardow, A. Life cycle assessment of CO₂-based C1-chemicals. *Green Chem.* **2017**, *19*, 2244–2259. [[CrossRef](#)]
12. Artz, J.; Müller, T.E.; Thenert, K.; Kleinekorte, J.; Meys, R.; Sternberg, A.; Bardow, A.; Leitner, W. Sustainable conversion of carbon dioxide: An integrated review of catalysis and life cycle assessment. *Chem. Rev.* **2018**, *118*, 434–504. [[CrossRef](#)]
13. Lee, J.S.; Jung, J.; Roh, K.; Heo, S.; Lee, U.; Lee, J.H. Risk-based uncertainty assessment to identify key sustainability hurdles for emerging CO₂ utilization technologies. *Green Chem.* **2022**, *24*, 4588–4605. [[CrossRef](#)]
14. Kim, C.; Lee, Y.; Kim, K.; Lee, U. Implementation of Formic Acid as a Liquid Organic Hydrogen Carrier (LOHC): Techno-Economic Analysis and Life Cycle Assessment of Formic Acid Produced via CO₂ Utilization. *Catalysts* **2022**, *12*, 1113. [[CrossRef](#)]
15. Guo, S.; Liu, Y.; Murphy, E.; Ly, A.; Xu, M.; Matanovic, I.; Pan, X.; Atanassov, P. Robust palladium hydride catalyst for electrocatalytic formate formation with high CO tolerance. *Appl. Catal. B-Environ.* **2022**, *316*, 121659. [[CrossRef](#)]
16. Koolen, C.D.; Luo, W.; Züttel, A. From single crystal to single atom catalysts: Structural factors influencing the performance of metal catalysts for CO₂ electroreduction. *ACS Catal.* **2022**, *13*, 948–973. [[CrossRef](#)]
17. Zhang, J.; Pham, T.H.M.; Ko, Y.; Li, M.; Yang, S.; Koolen, C.D.; Zhong, L.; Luo, W.; Züttel, A. Tandem effect of Ag@C@Cu catalysts enhances ethanol selectivity for electrochemical CO₂ reduction in flow reactors. *Cell Rep. Phys. Sci.* **2022**, *3*, 100949. [[CrossRef](#)]
18. Wang, W.; Wang, S.; Ma, X.; Gong, J. Recent advances in catalytic hydrogenation of carbon dioxide. *Chem. Soc. Rev.* **2011**, *40*, 3703–3727. [[CrossRef](#)] [[PubMed](#)]
19. Bulushev, D.A.; Ross, J.R. Heterogeneous catalysts for hydrogenation of CO₂ and bicarbonates to formic acid and formates. *Catal. Rev.* **2018**, *60*, 566–593. [[CrossRef](#)]

20. Yan, N.; Philippot, K. Transformation of CO₂ by using nanoscale metal catalysts: Cases studies on the formation of formic acid and dimethylether. *Curr. Opin. Chem. Eng.* **2018**, *20*, 86–92. [[CrossRef](#)]
21. Gunasekar, G.H.; Park, K.; Jung, K.-D.; Yoon, S. Recent developments in the catalytic hydrogenation of CO₂ to formic acid/formate using heterogeneous catalysts. *Inorg. Chem. Front.* **2016**, *3*, 882–895. [[CrossRef](#)]
22. Park, K.; Gunasekar, G.H.; Yoon, S. Heterogenized Catalyst for the Hydrogenation of CO₂ to Formic Acid or Its Derivatives. In *CO₂ Hydrogenation Catalysis*; Wiley: Hoboken, NJ, USA, 2021; pp. 149–177.
23. Sun, R.; Liao, Y.; Bai, S.-T.; Zheng, M.; Zhou, C.; Zhang, T.; Sels, B.F. Heterogeneous catalysts for CO₂ hydrogenation to formic acid/formate: From nanoscale to single atom. *Energy Environ. Sci.* **2021**, *14*, 1247–1285. [[CrossRef](#)]
24. Verma, P.; Zhang, S.; Song, S.; Mori, K.; Kuwahara, Y.; Wen, M.; Yamashita, H.; An, T. Recent strategies for enhancing the catalytic activity of CO₂ hydrogenation to formate/formic acid over Pd-based catalyst. *J. CO₂ Util.* **2021**, *54*, 101765. [[CrossRef](#)]
25. Ranade, V.V.; Chaudhari, R.; Gunjal, P.R. *Trickle Bed Reactors: Reactor Engineering and Applications*; Elsevier: Amsterdam, The Netherlands, 2011.
26. Saeidi, S.; Amin, N.A.S.; Rahimpour, M.R. Hydrogenation of CO₂ to value-added products—A review and potential future developments. *J. CO₂ Util.* **2014**, *5*, 66–81. [[CrossRef](#)]
27. Park, K.; Gunasekar, G.H.; Kim, S.-H.; Park, H.; Kim, S.; Park, K.; Jung, K.-D.; Yoon, S. CO₂ hydrogenation to formic acid over heterogenized ruthenium catalysts using a fixed bed reactor with separation units. *Green Chem.* **2020**, *22*, 1639–1649. [[CrossRef](#)]
28. Ahn, S.; Park, K.; Lee, K.R.; Haider, A.; Van Nguyen, C.; Jin, H.; Yoo, S.J.; Yoon, S.; Jung, K.-D. Atomically dispersed Ru (III) on N-doped mesoporous carbon hollow spheres as catalysts for CO₂ hydrogenation to formate. *Chem. Eng. J.* **2022**, *442*, 136185. [[CrossRef](#)]
29. Kim, C.; Park, K.; Lee, H.; Im, J.; Usosky, D.; Tak, K.; Park, D.; Chung, W.; Han, D.; Yoon, J. Accelerating the net-zero economy with CO₂-hydrogenated formic acid production: Process development and pilot plant demonstration. *Joule* **2024**. [[CrossRef](#)]
30. Fagherazzi, G.; Benedetti, A.; Polizzi, S.; Di Mario, A.; Pinna, F.; Signoreto, M.; Pernicone, N. Structural investigation on the stoichiometry of β-PdH_x in Pd/SiO₂ catalysts as a function of metal dispersion. *Catal. Lett.* **1995**, *32*, 293–303. [[CrossRef](#)]
31. Iwasa, N.; Mayanagi, T.; Ogawa, N.; Sakata, K.; Takezawa, N. New catalytic functions of Pd–Zn, Pd–Ga, Pd–In, Pt–Zn, Pt–Ga and Pt–In alloys in the conversions of methanol. *Catal. Lett.* **1998**, *54*, 119–123. [[CrossRef](#)]
32. Bardestani, R.; Patience, G.S.; Kaliaguine, S. Experimental methods in chemical engineering: Specific surface area and pore size distribution measurements—BET, BJH, and DFT. *Can. J. Chem. Eng.* **2019**, *97*, 2781–2791. [[CrossRef](#)]
33. Niu, Y.; Liu, X.; Wang, Y.; Zhou, S.; Lv, Z.; Zhang, L.; Shi, W.; Li, Y.; Zhang, W.; Su, D.S. Visualizing formation of intermetallic PdZn in a palladium/zinc oxide catalyst: Interfacial fertilization by PdH_x. *Angew. Chem. Int. Ed.* **2019**, *58*, 4232–4237. [[CrossRef](#)]
34. Gniewek, A.; Trzeciak, A.M.; Ziółkowski, J.J.; Kępiński, L.; Wrzyszczyk, J.; Tylus, W. Pd-PVP colloid as catalyst for Heck and carbonylation reactions: TEM and XPS studies. *J. Catal.* **2005**, *229*, 332–343. [[CrossRef](#)]
35. Vanni, M.; Bellini, M.; Borsacchi, S.; Calucci, L.; Caporali, M.; Caporali, S.; d’Acapito, F.; Geppi, M.; Giaccherini, A.; Ienco, A. Interlayer Coordination of Pd–Pd Units in Exfoliated Black Phosphorus. *J. Am. Chem. Soc.* **2021**, *143*, 10088–10098. [[CrossRef](#)] [[PubMed](#)]
36. Dobrovolskaya, A.V.; Chapek, S.V.; Usoltsev, O.A.; Naranov, E.; Gorbunov, D.N.; Trigub, A.L.; Maximov, A.L.; Soldatov, A.V.; Bugaev, A.L. High-Quality In Situ X-ray Absorption Spectroscopy Monitoring of the Palladium Nucleation inside the 3D Printed Microfluidic Chip. *J. Phys. Chem. C* **2023**, *127*, 20727–20733. [[CrossRef](#)]
37. Chen, B.F.; Dong, M.H.; Liu, S.L.; Xie, Z.B.; Yang, J.J.; Li, S.P.; Wang, Y.Y.; Du, J.; Liu, H.Z.; Han, B.X. CO₂ Hydrogenation to Formate Catalyzed by Ru Coordinated with a N,P-Containing Polymer. *ACS Catal.* **2020**, *10*, 8557–8566. [[CrossRef](#)]
38. Zhang, Z.; Zhang, L.; Hülsey, M.J.; Yan, N. Zirconia phase effect in Pd/ZrO₂ catalyzed CO₂ hydrogenation into formate. *Mol. Catal.* **2019**, *475*, 110461. [[CrossRef](#)]
39. Zhang, Z.; Zhang, L.; Yao, S.; Song, X.; Huang, W.; Hülsey, M.J.; Yan, N. Support-dependent rate-determining step of CO₂ hydrogenation to formic acid on metal oxide supported Pd catalysts. *J. Catal.* **2019**, *376*, 57–67. [[CrossRef](#)]
40. Yang, G.; Kuwahara, Y.; Mori, K.; Louis, C.; Yamashita, H. PdAg alloy nanoparticles encapsulated in N-doped microporous hollow carbon spheres for hydrogenation of CO₂ to formate. *Appl. Catal. B-Environ.* **2021**, *283*, 119628. [[CrossRef](#)]
41. Yang, G.; Kuwahara, Y.; Mori, K.; Louis, C.; Yamashita, H. Pd-Cu Alloy Nanoparticles Confined within Mesoporous Hollow Carbon Spheres for the Hydrogenation of CO₂ to Formate. *J. Phys. Chem. C* **2021**, *125*, 3961–3971. [[CrossRef](#)]
42. Mori, K.; Hata, H.; Yamashita, H. Interplay of Pd ensemble sites induced by GaO_x modification in boosting CO₂ hydrogenation to formic acid. *Appl. Catal. B-Environ.* **2023**, *320*, 122022. [[CrossRef](#)]
43. Park, K.; Lee, K.R.; Ahn, S.; Kim, S.H.; Haider, A.; Choung, S.; Han, J.W.; Jung, K.D. Structural effects of nitrogen-doped titanium oxide supports on stabilization of ruthenium active species in carbon dioxide hydrogenation to formate. *Appl. Catal. B-Environ.* **2023**, *335*, 122873. [[CrossRef](#)]
44. Park, K.; Lee, K.R.; Ahn, S.; Van Nguyen, C.; Jung, K.-D. Effects of the chemical states of N sites and mesoporosity of N-doped carbon supports on single-atom Ru catalysts during CO₂-to-formate conversion. *Appl. Catal. B-Environ.* **2024**, *346*, 123751. [[CrossRef](#)]

Disclaimer/Publisher’s Note: The statements, opinions and data contained in all publications are solely those of the individual author(s) and contributor(s) and not of MDPI and/or the editor(s). MDPI and/or the editor(s) disclaim responsibility for any injury to people or property resulting from any ideas, methods, instructions or products referred to in the content.